IT'IS FOUNDATION

Foundation for Research on Information Technologies in Society

Prof. Dr. Niels Kuster

Director Foundation IT'IS
Professor of Swiss Federal Institute of Technology – ETHZ
Phone +41 1 245 9690 · kuster@itis.ethz.ch

Project 594B

Dosimetric Assessment of the Kathrein In-Ground Antenna (TN: 80010233 / SN: D714407561)

(Numerical Study)

Eugenia Cabot, Beyhan Kochali, and Sven Kuehn

Zurich, January 2016

Executive Summary

The numerical model of the Kathrein In-Ground Antenna prototype from Swisscom Ltd. was developed from the CAD model provided by Swisscom and validated with measurements. The validation of the numerical model was performed by comparison with specific absorption rate (SAR) measurements made inside the elliptical phantom ELI4 filled with 'HBBL600-6000V6' tissue simulating liquid. The phantom was exposed to the antenna at three different distances. The model validation was within 0.4 dB for a κ = 2 uncertainty of 0.94 dB.

The validated numerical model was then used to assess human exposure to the antenna. The assessment of human exposure was performed for two scenarios: an adult male standing on top of the antenna and a 3-year-old child sitting on top of the antenna. In summary, the maximum SAR values in the human models exposed to the device are summarized in Table 1. The maximum SAR values were obtained after sweeping the phase of the two input ports, and only the worst case is reported in Table 1. For the remaining cases, refer to the summaries in Tables 8 and 9 in the report. All values are given for 1 W forward power at each antenna external feed port, i.e., 2 W total input power.

Model	**Freq.** (GHz)	**wbSAR (W/kg)/(2·W)**	**SAR10g (W/kg)/(2·W)**
Duke	1.82	0.0045 ± 0.96 dB	0.88 ± 0.96 dB
Nina	1.82	0.033 ± 0.96 dB	0.90 ± 0.96 dB
Duke	2.655	0.0032 ± 0.96 dB	0.63 ± 0.96 dB
Nina	2.655	0.021 ± 0.96 dB	0.70 ± 0.96 dB

Table 1: Worst case peak SAR10g in the human models. All values are given for 1 W forward power at each antenna feed port, i.e., 2 W total input power.

Both human model scenarios yielded results that indicate exposure below the SAR limits for the general public, for whole body SAR (wbSAR) and 10 g averaged SAR (SAR10g), according to the Basic Restrictions for Peak Average SAR of the International Commission on Non-Ionizing Radiation Protection (ICNIRP) "Guidelines for Limiting Exposure to Time-Varying Electric, Magnetic, and Electromagnetic Fields (up to 300 GHz)" [1] for 1 W at each antenna external feed port, i.e., 2 W total input power.

Contents

1 Introduction and Objectives

The objective of this project was to perform a SAR evaluation of the Kathrein In-Ground Antenna prototype from Swisscom Ltd. This report focuses on the numerical evaluation of the antenna, which consisted of:

- Validation of the numerical antenna model configured as for the measurements. The elliptical flat phantom filled with tissue simulating liquid was exposed to the antenna fields. The comparison of the numerical and experimental results was performed.
- SAR simulation of an adult human standing on top of the antenna and assessment of the compliance with safety limits for localized and whole-body averaged SAR.
- SAR simulation of a young child sitting on top of the antenna and assessment of the compliance with safety limits for localized and whole-body averaged SAR.
- MIMO evaluation of the antenna loaded with the human models listed above.

The following sections summarize the work performed to achieve these goals.

2 Methods

Swisscom provided the CAD file of the antenna model used for the simulations. The model is shown in Figure 1. All numerical computations were performed with SEMCAD X 14.8, an FDTD based platform developed by SPEAG. The simulation sets can be separated into two groups:

- Antenna with the ELI4 phantom: simulations were performed with the elliptical ELI4 phantom filled of tissue simulating liquid and the antenna positioned at three distances from the bottom of the phantom: 0, 5, and 10 mm. The simulations were performed at 2 frequencies: 1.82 and 2.655 GHz.
- Antenna with human models: Simulations were performed with the antenna and two human models. An adult male model standing on top of the antenna and a 3-year-old child sitting on top of the antenna were selected as exposure scenarios. The simulations were run at two frequencies: 1.82 and 2.655 GHz.

The antenna has two accessible external feed ports. Each of these ports is connected through a feeding network to two internal feed points, named here as S1, S2, S3, and S4. The position of the internal ports with respect to the phantom is shown in Figure 1(b). One external port is linked to source points S1 and S3, whereas the other port is linked to S2 and S4. The simulations are run for S1 and S3 active (with S2 and S4 loaded with a 50 Ω load), or for S2 and S4 active (with S1 and S3 loaded with a 50 Ω load). No phase difference was applied to the internal feed point pairs S1S3 and S2S4.

Simulation Port Power. Let the power at the S1 and S3 ports be P_{S1} and P_{S3}, respectively, and P_1 the power at the external port 1. The equation $P_{S1} + P_{S3} + P_{loss} = P_1$ would describe how the inner and outer ports are related, with P_{loss} the power loss of the internal feed network from the external to the internal ports. Reciprocally for the other pair of internal ports S2S4, the equation $P_{S2} + P_{S4} + P_{loss} = P_2$ would apply.

3 Validation of the Antenna Model

3.1 Antenna and ELI4 Phantom

Harmonic simulations at 1.82 and 2.655 GHz have been performed for the antenna positioned at three different distances from the ELI4 phantom: 0, 5, and 10 mm (see Figure 2). The ELI4 phantom content has been assigned the properties of the 'HBBL600-6000V6' liquid, i.e. $\epsilon_r = 41$ and $\sigma = 1.41$ S/m at 1.82 GHz, and $\epsilon_r = 40.9$ and $\sigma = 2$ S/m at 2.655 GHz, with density $\rho = 1000\,\mathrm{kg/m^3}$. The parameters of the antenna components have been assigned as specified by Swisscom. In the measurement setup the antenna was

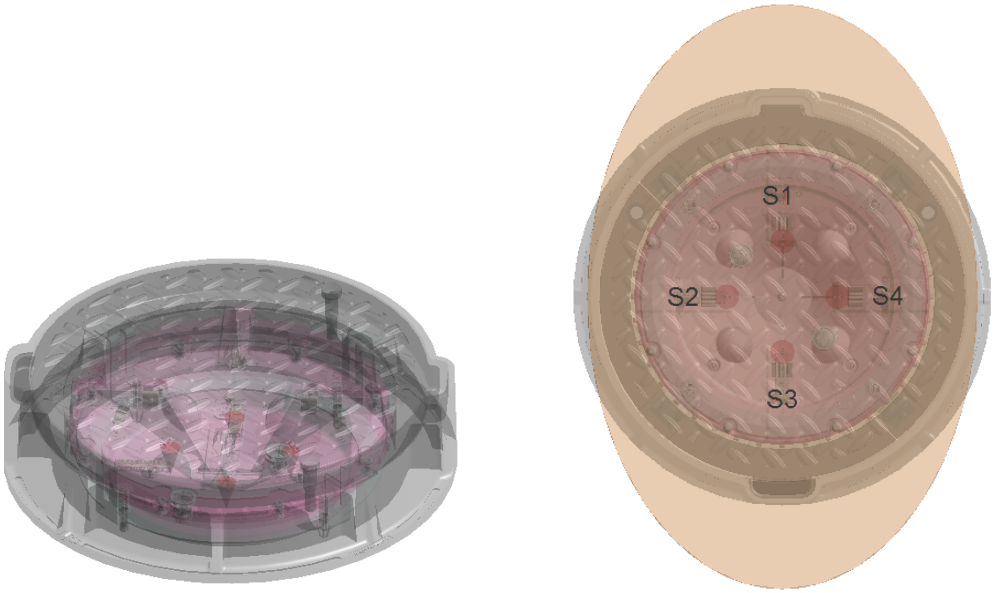

(a) Antenna (b) Top view of antenna and ELI4 phantom

Figure 1: Antenna model (1(a)) and position of the inner feed points with respect to the ELI4 phantom (1(b)).

positioned on top of a metal table, which was also added to the simulations. The concrete layers and the soil surrounding the antenna model have not been used in the simulations involving the ELI4 phantom, since they were not present in the measurement setup either.

The results of the SAR assessment are summarized in Table 2. Plots of the SAR distributions are shown in Appendix A. All the results are given for 1 W antenna external feed port forward power.

Phantom	**Frequency (GHz)**	**Distance (mm)**	**SAR10g S1 S3 (W/kg)/W**	**SAR10g S2 S4 (W/kg)/W**
ELI4 flat	1.82	0	0.59	0.58
ELI4 flat	1.82	5	0.54	0.6
ELI4 flat	1.82	10	0.56	0.59
ELI4 flat	2.655	0	0.37	0.39
ELI4 flat	2.655	5	0.28	0.38
ELI4 flat	2.655	10	0.28	0.28

Table 2: Results of the SAR assessment at 1.82 and 2.655 GHz, for the antenna at three distances from the bottom of the ELI4 phantom. All values are given for 1 W antenna external feed port forward power.

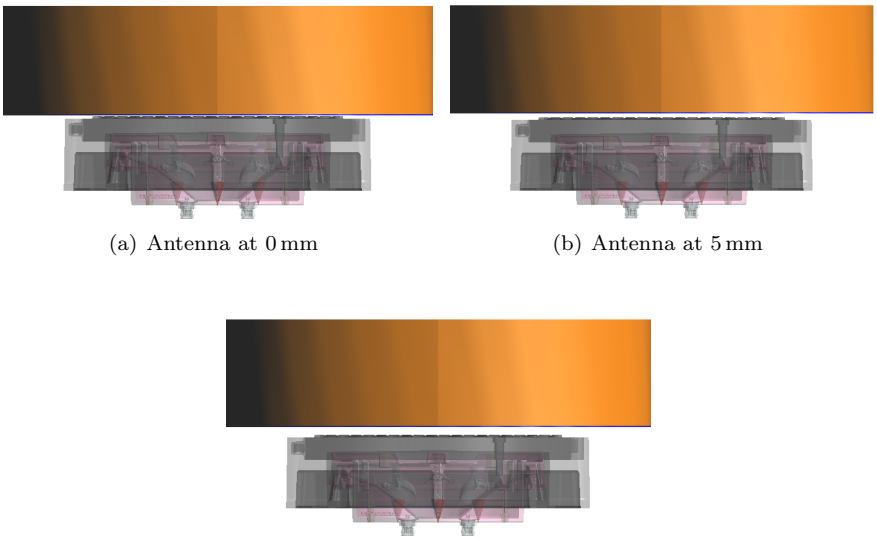

(a) Antenna at 0 mm (b) Antenna at 5 mm

(c) Antenna at 10 mm

Figure 2: Side view of the antenna position with respect to the ELI4 phantom at each distance.

3.2 Uncertainty Assessment

The uncertainty for the numerical simulations of the antenna with the ELI4 phantom was assessed and is summarized in Table 3. The expanded uncertainty ($\kappa = 2$) is estimated to be 0.94 dB.

The total combined uncertainty (numerical and experimental) is summarized in Table 4. The expanded total combined uncertainty ($\kappa = 2$) is estimated to be 1.28 dB.

Uncertainty Component	**Tolerance (dB)** SAR10g	**Prob. Dist.**	**Div.**	c_i	**Std. Unc (dB)** SAR10g
Simulation Time	0	N	1	1	0
Absorbing Boundaries	0	N	1	1	0
ELI4 Liquid Permittivity	0.073	N	1	1	0.073
ELI4 Liquid Conductivity	0.052	N	1	1	0.052
ELI4 Liquid Permittivity (Manufacturing)	0.304	N	1	1	0.304
ELI4 Liquid Conductivity (Manufacturing)	0.104	N	1	1	0.104
Grid	0.20	N	1	1	0.20
Representation of Device	0.26	N	1	1	0.26
Combined Standard Unc.		**RSS**			0.47
Expanded Unc. ($\kappa = 2$)					0.94

Table 3: Uncertainty budget for the simulations with the antenna and the ELI4 flat phantom.

Uncertainty Component	**Tolerance (dB)** SAR10g	**Prob. Dist.**	**Div.**	c_i	**Std. Unc (dB)** SAR10g
Combined Numerical Unc.	0.47	N	1	1	0.47
Combined Experimental Unc.	0.43	N	1	1	0.43
Total Combined Standard Unc.		**RSS**			0.64
Expanded Unc. ($\kappa = 2$)					1.28

Table 4: Total combined numerical and experimental uncertainty of the SAR assessment with the ELI4 phantom.

3.3 Validation

The values of the peak SAR averaged over 10 g obtained with measurements and simulations are summarized in Table 5 for the three distances of the antenna to the phantom. The deviations of simulations with respect to measurements in dB, also listed in Table 5, deviations are all within 0.4 dB. For each validation case, the deviation between the simulated value and the measured value is lower than the expanded combined uncertainties, i.e., the RSS of the numerical uncertainty and measurement uncertainty (1.28 dB, see Table 4) and, therefore, the antenna model can be considered validated.

Phantom	**Freq.** (GHz)	**Dist.** (mm)	Sim. **SAR10g S1 S3** (W/kg)/W	Sim. **SAR10g S2 S4** (W/kg)/W	Meas. **SAR10g S1 S3** (W/kg)/W	Meas. **SAR10g S2 S4** (W/kg)/W	**Deviation S1 S3** (dB)	**Deviation S2 S4** (dB)
ELI4 flat	1.82	0	0.59	0.58	0.56	0.6	0.24	-0.11
ELI4 flat	1.82	5	0.54	0.6	0.58	0.59	-0.28	0.084
ELI4 flat	1.82	10	0.56	0.59	0.57	0.57	-0.09	0.18
ELI4 flat	2.655	0	0.37	0.39	0.38	0.39	-0.057	0.013
ELI4 flat	2.655	5	0.28	0.38	0.31	0.36	-0.39	0.32
ELI4 flat	2.655	10	0.28	0.28	0.28	0.27	0.03	0.12

Table 5: SAR10g values obtained experimentally and numerically, and deviation from measurement and simulation in dB. The deviations are computed from the non-rounded values of SAR.

4 Human Exposure Assessment

4.1 Human Exposure to Single Port Configurations

For the assessment of the absorption in humans due to exposure to the antenna, two scenarios were selected: an adult standing on the antenna and a child sitting on the antenna. The characteristics of Duke (adult male) and Nina (three-year-old girl) are summarized in Table 6.

For the positioning of the human models, the poser tool in SEMCAD was used. To have maximum surface contact of the feet of the adult male with the antenna, the feet were repositioned by turning them by 15 degrees around the ankle axis with the poser tool. The child model was positioned to sit with legs stretched on top of the antenna. Figure 3 shows the setups used in the simulations to assess the exposure of the human models to the antenna. The dielectric properties of the human models at the corresponding frequency are set according to the material database in [2]. The layers of soil and concrete surrounding the antenna have been included in the simulations involving the human models. The antenna materials are set as indicated by Swisscom, except for concrete, which was not specified. The dielectric properties of concrete were taken from [3]. Specifically, air-dried concrete, with a permittivity $\epsilon_r = 5$ with negligible conductivity at both 1.82 and 2.655 GHz, was used.

The peak 10g spatial average SAR, as well as the whole body SAR (wbSAR), i.e. power absorbed in the whole body divided by the total body mass, are summarized in Table 7. Both the wbSAR and the SAR10g are below the limits for the general public exposure (0.08 W/kg and 2 W/kg respectively) for both models, for 1 W forward power at the external port. The peak SAR10g value obtained for Nina at the highest frequency is considerably larger than the homogeneous case for one of the port configurations. This can be explained by the layering effect of tissues, which can exhibit enhancement of absorption compared to the homogeneous case, as has been extensively studied in the past, for instance in [4].

Figure 4 shows the distribution of the SAR averaged over 10 g at the slice where the maximum occurs for both models. The red cube indicates the position of the peak SAR volume.

	Duke	**Nina**
sex	male	female
age [y]	34	3
height [m]	1.77	0.916
weight [kg]	72.41	13.9
BMI [kg/m^2]	23.06	16.6

Table 6: Characteristics of the human models used in this study.

Model	**Freq.** (GHz)	**wbSAR S1 S3 (W/kg)/W**	**wbSAR S2 S4 (W/kg)/W**	**SAR10g S1 S3 (W/kg)/W**	**SAR10g S2 S4 (W/kg)/W**
Duke	1.82	0.0041	0.0044	0.65	0.64
Nina	1.82	0.028	0.026	0.66	0.58
Duke	2.655	0.0023	0.0024	0.48	0.42
Nina	2.655	0.020	0.013	0.68	0.36

Table 7: Results of the wbSAR and peak SAR10g obtained for the human models. All values are given for 1 W antenna external feed port forward power.

4.2 MIMO Evaluation

In the previous section, the exposure of the human models to the single port driven antenna was evaluated. In reality, the antenna would be fed at both ports, with a certain amplitude and phase difference applied to the two input signals. To ascertain which combination yields the worst case peak SAR10g, a sweep of the

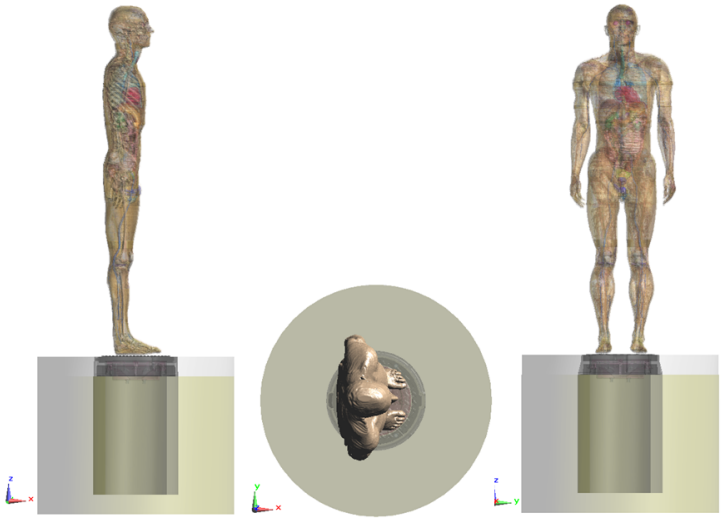

(a) Duke

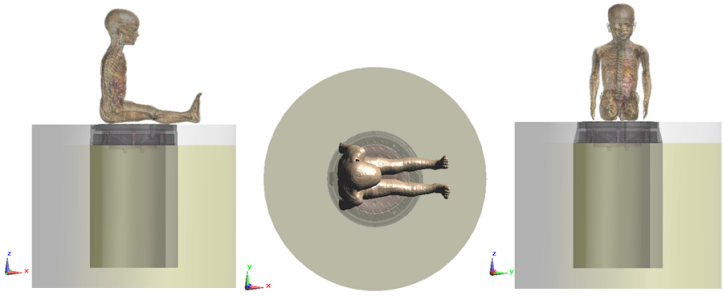

(b) Nina

Figure 3: Position of the human models with respect to the antenna (side, top, and front views).

amplitude and phase of the single ports needs to be performed. For each amplitude/phase combination, the single port induced fields in the human models were combined, and the resulting peak SAR10g computed. The phase difference has been swept in 45° steps and the amplitudes of both ports have been fixed to 1 W each. The results can be scaled to a different power as long as the differential power stays 1:1 between the ports. The resulting peak SAR10g values for Duke and Nina are summarized in Table 8. For the two models, the maximum peak SAR10g is obtained for a phase difference between the two ports of 180°, at both working frequencies. At the lower frequency, the maximum values of peak SAR10g were 0.88 and 0.90 W/kg for Duke and Nina, respectively, whereas, at the highest frequency, the values were 0.63 (Duke) and 0.70 W/kg (Nina).

Table 9 contains the values of the SAR averaged over the total body mass obtained for the phase sweep. The maximum values obtained for Duke were 0.0045 W/kg and 0.0032 W/kg, for 1.82 and 2.655 GHz, respectively. As for Nina, the maximum values for the wbSAR were 0.033 W/kg (1.82 GHz) and 0.021 W/kg (2.655 GHz). All reported values are given for an input power of 1 W at each external port, i.e. 2 W total input power.

4.3 Uncertainty Assessment

The uncertainty for the numerical simulations of the antenna with the human models was assessed and is summarized in Table 10. The expanded uncertainty ($\kappa = 2$) is estimated to be 0.96 dB.

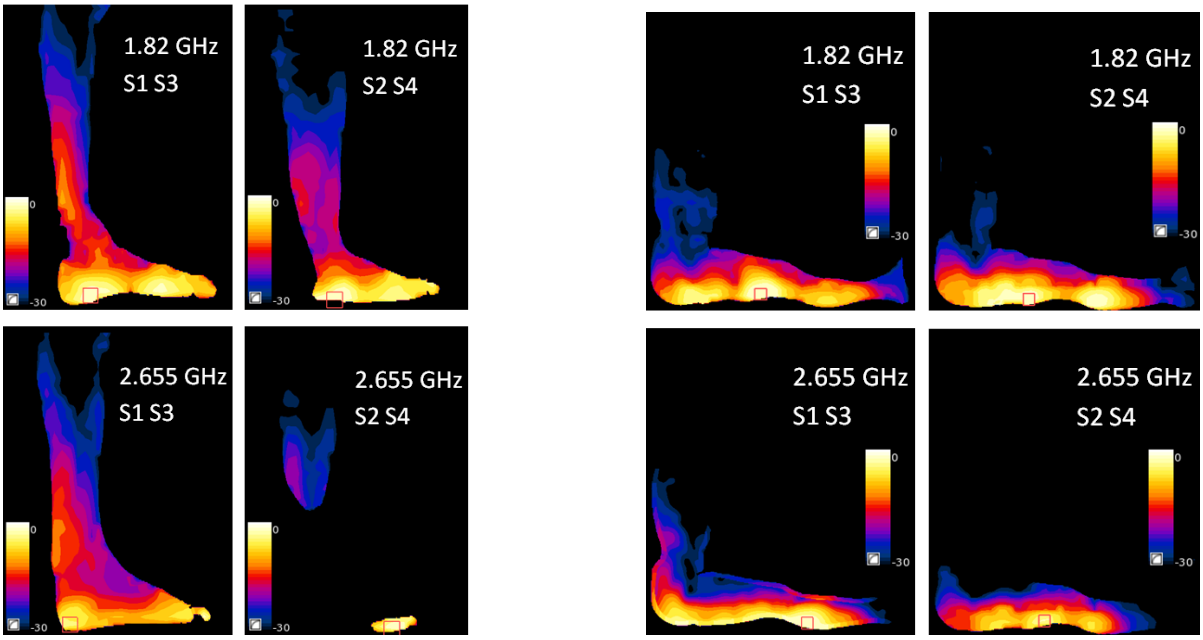

Figure 4: Distribution of the SAR averaged over 10 g for the human models at the slice containing the maximum value. The red cube indicates the location of the peak SAR volume. The 0 dB in the scale corresponds to 0.5 W/kg, for 1 W antenna external feed port forward power.

Model	**Freq. (GHz)**	**Power (per port) (W)**	**SAR10g (W/kg)/(2·W) for different phase**							
			0°	45°	90°	135°	180°	225°	270°	315°
Duke	1.82	1	0.61	0.83	0.72	0.84	**0.88**	0.76	0.58	0.59
Nina	1.82	1	0.55	0.59	0.61	0.84	**0.90**	0.82	0.63	0.58
Duke	2.655	1	0.59	0.51	0.42	0.55	**0.63**	0.54	0.39	0.54
Nina	2.655	1	0.57	0.59	0.53	0.65	**0.70**	0.56	0.47	0.55

Table 8: Peak SAR10g resulting from the combination of the single port fields for phase sweep in 45° steps. Maximum values are bold.

Model	**Freq. (GHz)**	**Power (per port) (W)**	**wbSAR (W/kg)/(2·W) for different phase**							
			0°	45°	90°	135°	180°	225°	270°	315°
Duke	1.82	1	0.0040	0.0042	0.0044	**0.0045**	0.0044	0.0042	0.0040	0.0040
Nina	1.82	1	0.022	0.026	0.030	0.033	**0.033**	0.029	0.024	0.021
Duke	2.655	1	0.0019	0.0020	0.0024	0.0029	**0.0032**	0.0031	0.0027	0.0022
Nina	2.655	1	0.013	0.015	0.019	0.021	**0.021**	0.019	0.016	0.013

Table 9: wbSAR resulting from the combination of the single port fields for phase sweep in 45° steps.

Uncertainty Component	**Tolerance (dB)** SAR10g	**Prob. Dist.**	**Div.**	c_i	**Std. Unc (dB)** SAR10g
Simulation Time	0	N	1	1	0
Absorbing Boundaries	0	N	1	1	0
Tissue Properties Permittivity	0.57	R	1.73	1	0.34
Tissue Properties Conductivity	0.21	R	1.73	1	0.12
Grid	0.17	N	1	1	0.17
Representation of Device	0.26	N	1	1	0.26
Combined Standard Unc.		**RSS**			0.48
Expanded Unc. ($\kappa = 2$)					0.96

Table 10: Uncertainty budget for the simulations with the antenna and the human models.

5 Conclusions

The numerical model of the Kathrein In-Ground Antenna prototype from Swisscom Ltd. was developed from the CAD model provided by Swisscom and validated with measurements. The validation of the model was done by comparison with SAR measurements made inside the elliptical phantom ELI4 filled with tissue simulating liquid, exposed to the antenna at three different distances from the phantom, and at two frequencies. Simulations were performed with one port active and the other port terminated with a 50 Ω load, alternating the active port. The model validation was within 0.4 dB for a $\kappa = 2$ uncertainty of 0.94 dB.

The validated numerical model was then used to assess the human exposure to the antenna. The assessment of the human exposure was performed for two scenarios: an adult male standing on top of the antenna and a 3-year-old child sitting on top of the antenna. In both cases, results indicate human exposures below the SAR limits for exposure of the general public in terms of both wbSAR and 10 g averaged SAR, according to the Basic Restrictions for Peak Average SAR of the International Commission on Non-Ionizing Radiation Protection (ICNIRP) [1] for 1 W forward power at the antenna feed port.

A SAR Distributions in the ELI4 Phantom

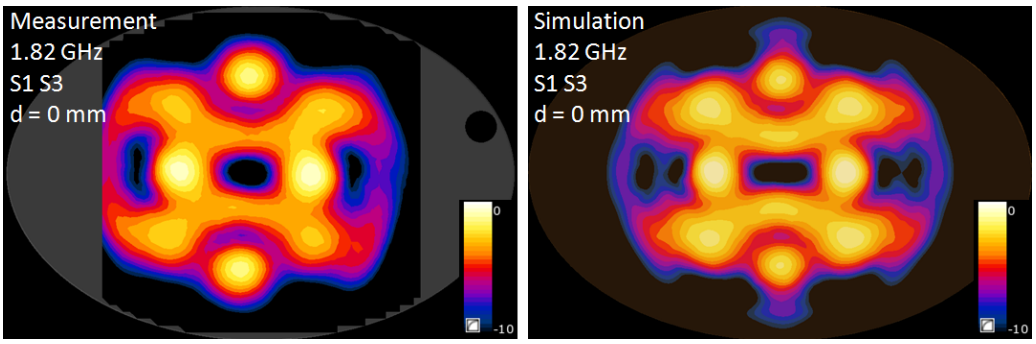

Figure 5: SAR distribution at 2.5 mm from the bottom of the ELI4 phantom with the antenna at 0 mm distance below the phantom ($f = 1.82$ GHz). The active feed points are S1 and S3. S2 and S4 are loaded with a 50 Ω load. 0 dB corresponds to 1.1 W/kg, for 1 W forward power at the active external port.

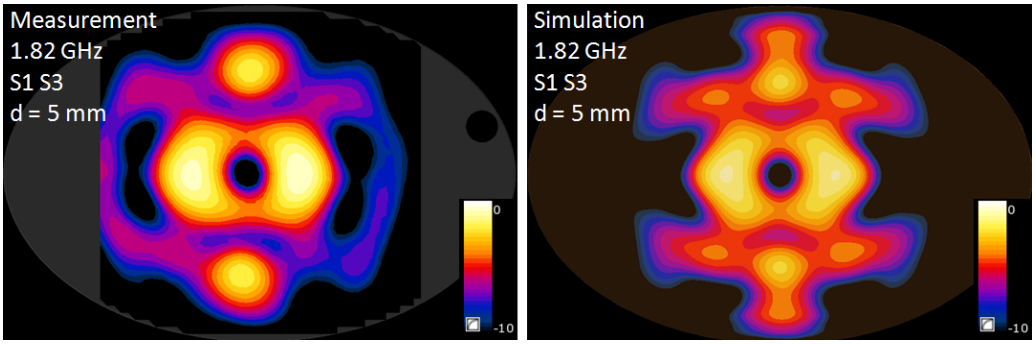

Figure 6: SAR distribution at 2.5 mm from the bottom of the ELI4 phantom with the antenna at 5 mm distance below the phantom ($f = 1.82$ GHz). The active feed points are S1 and S3. S2 and S4 are loaded with a 50 Ω load. 0 dB corresponds to 1.1 W/kg, for 1 W forward power at the active external port.

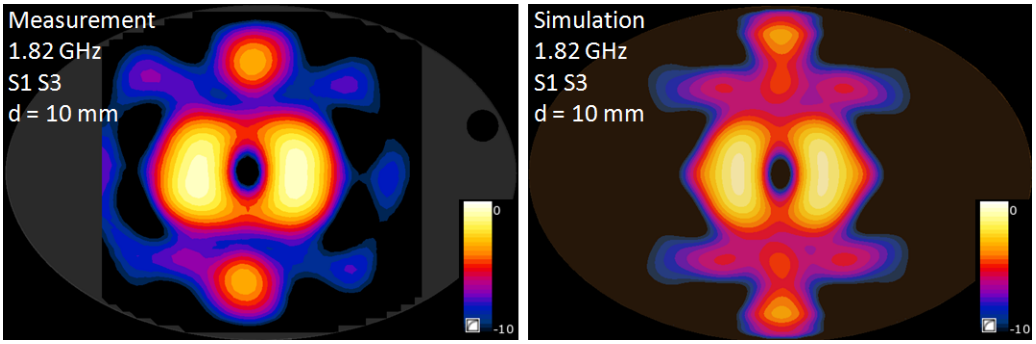

Figure 7: SAR distribution at 2.5 mm from the bottom of the ELI4 phantom with the antenna at 10 mm distance below the phantom ($f = 1.82$ GHz). The active feed points are S1 and S3. S2 and S4 are loaded with a 50 Ω load. 0 dB corresponds to 1.1 W/kg, for 1 W forward power at the active external port.

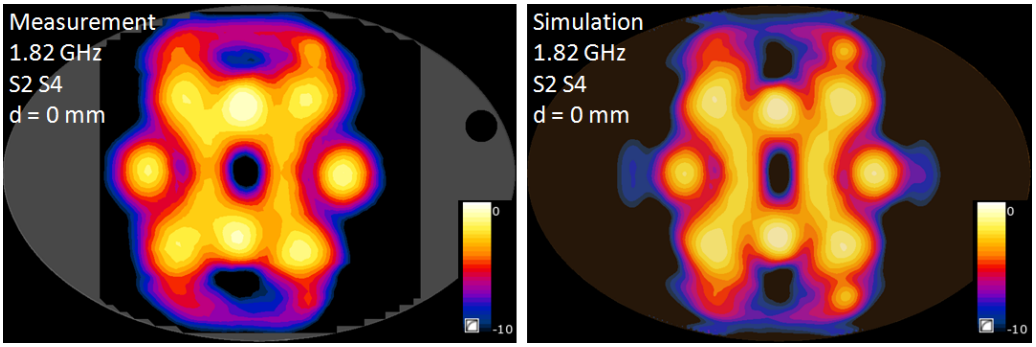

Figure 8: SAR distribution at 2.5 mm from the bottom of the ELI4 phantom with the antenna at 0 mm distance below the phantom ($f = 1.82$ GHz). The active feed points are S2 and S4. S1 and S3 are loaded with a 50 Ω load. 0 dB corresponds to 1.1 W/kg, for 1 W forward power at the active external port.

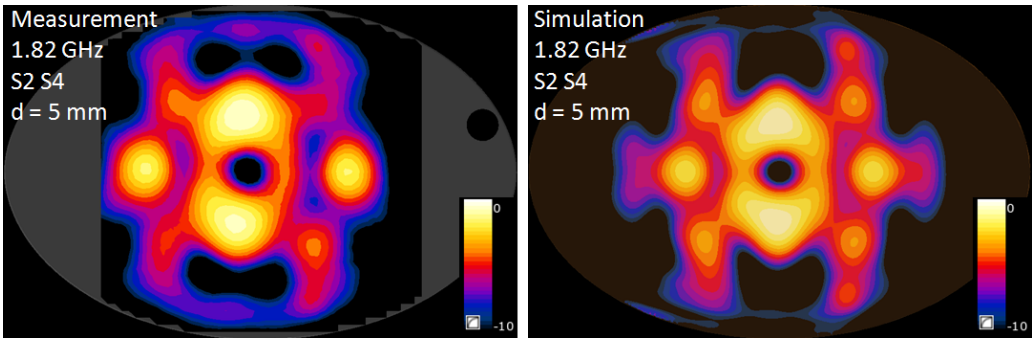

Figure 9: SAR distribution at 2.5 mm from the bottom of the ELI4 phantom with the antenna at 5 mm distance below the phantom ($f = 1.82$ GHz). The active feed points are S2 and S4. S1 and S3 are loaded with a 50 Ω load. 0 dB corresponds to 1.1 W/kg, for 1 W forward power at the active external port.

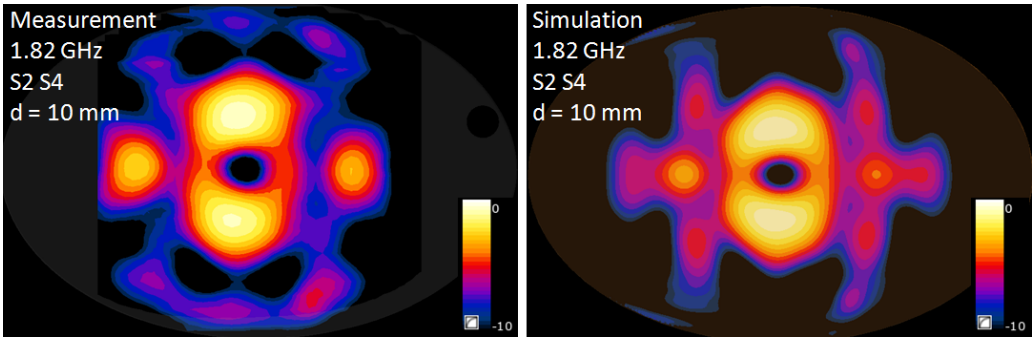

Figure 10: SAR distribution at 2.5 mm from the bottom of the ELI4 phantom with the antenna at 10 mm distance below the phantom ($f = 1.82$ GHz). The active feed points are S2 and S4. S1 and S3 are loaded with a 50 Ω load. 0 dB corresponds to 1.1 W/kg, for 1 W forward power at the active external port.

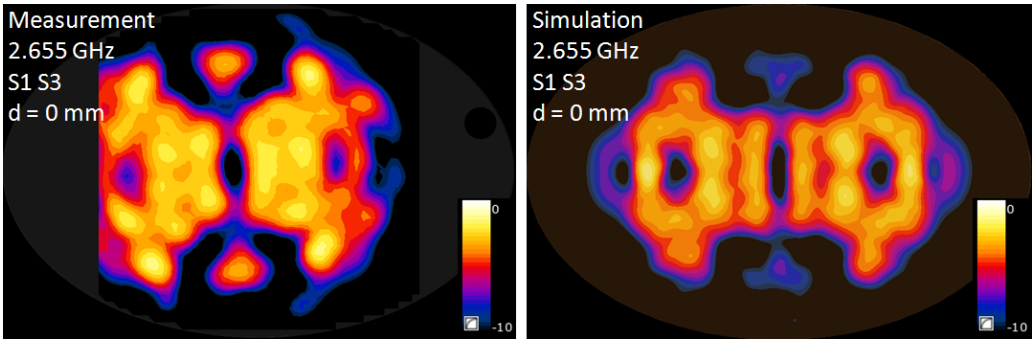

Figure 11: SAR distribution at 2.5 mm from the bottom of the ELI4 phantom with the antenna at 0 mm distance below the phantom ($f = 2.655$ GHz). The active feed points are S1 and S3. S2 and S4 are loaded with a 50 Ω load. 0 dB corresponds to 1.1 W/kg, for 1 W forward power at the active external port.

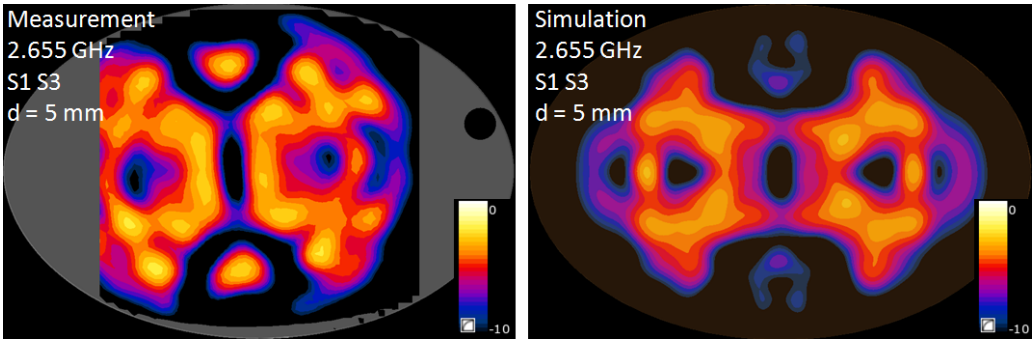

Figure 12: SAR distribution at 2.5 mm from the bottom of the ELI4 phantom with the antenna at 5 mm distance below the phantom ($f = 2.655$ GHz). The active feed points are S1 and S3. S2 and S4 are loaded with a 50 Ω load. 0 dB corresponds to 1.1 W/kg, for 1 W forward power at the active external port.

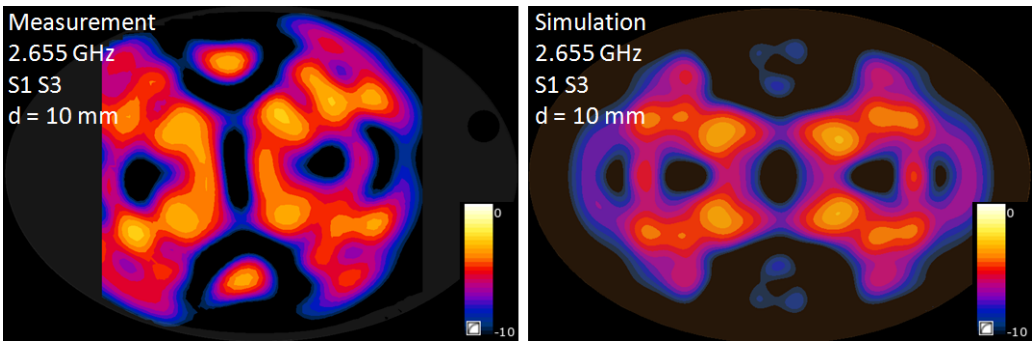

Figure 13: SAR distribution at 2.5 mm from the bottom of the ELI4 phantom with the antenna at 10 mm distance below the phantom ($f = 2.655$ GHz). The active feed points are S1 and S3. S2 and S4 are loaded with a 50 Ω load. 0 dB corresponds to 1.1 W/kg, for 1 W forward power at the active external port.

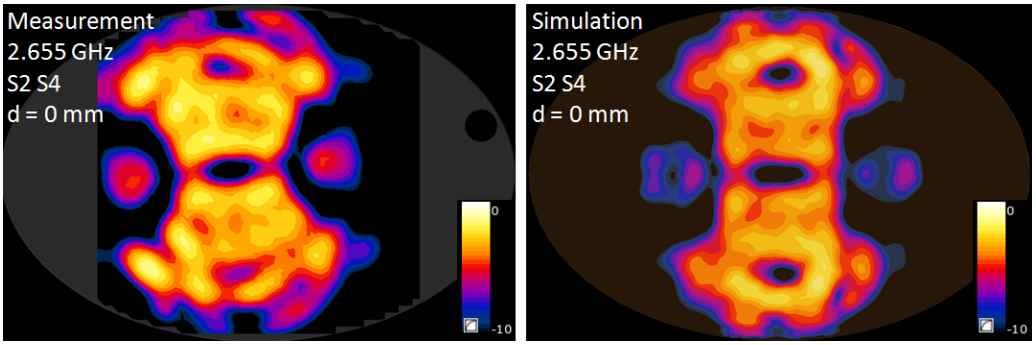

Figure 14: SAR distribution at 2.5 mm from the bottom of the ELI4 phantom with the antenna at 0 mm distance below the phantom ($f = 2.655$ GHz). The active feed points are S2 and S4. S1 and S3 are loaded with a 50 Ω load. 0 dB corresponds to 1.1 W/kg, for 1 W forward power at the active external port.

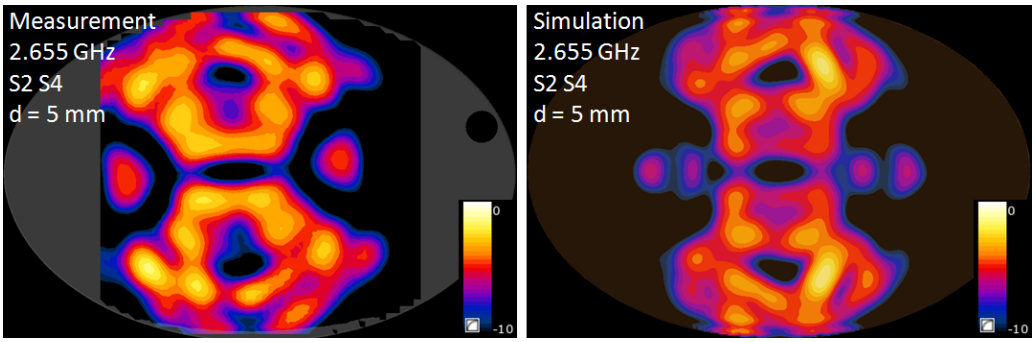

Figure 15: SAR distribution at 2.5 mm from the bottom of the ELI4 phantom with the antenna at 5 mm distance below the phantom ($f = 2.655$ GHz). The active feed points are S2 and S4. S1 and S3 are loaded with a 50 Ω load. 0 dB corresponds to 1.1 W/kg, for 1 W forward power at the active external port.

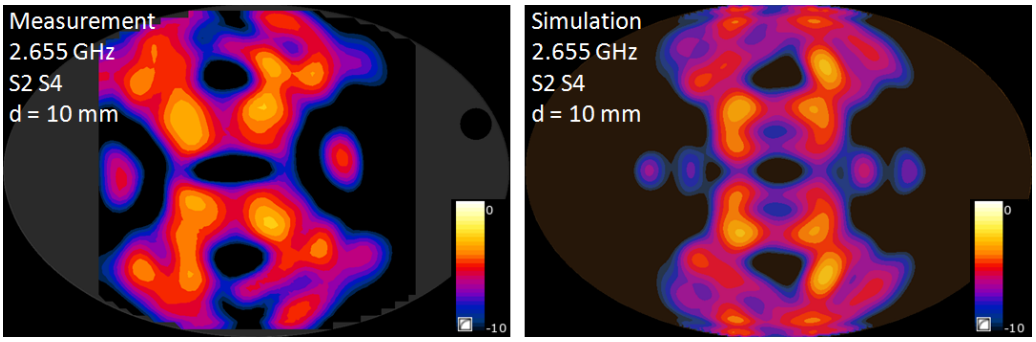

Figure 16: SAR distribution at 2.5 mm from the bottom of the ELI4 phantom with the antenna at 10 mm distance below the phantom ($f = 2.655$ GHz). The active feed points are S2 and S4. S1 and S3 are loaded with a 50 Ω load. 0 dB corresponds to 1.1 W/kg, for 1 W forward power at the active external port.

References

[1] ICNIRP. Guidelines for limiting exposure to time-varying electric, magnetic and electromagnetic fields (up to 300 GHz). Health Physics, 74:494–522, 1998.

[2] P.A. Hasgall, F. Di Gennaro, C. Baumgartner, E. Neufeld, M.C. Gosselin, D. Payne, A. Klingenböck, and N. Kuster. "IT'IS database for thermal and electromagnetic parameters of biological tissues", DOI: 10.13099/vip21000-03-0. September 2015.

[3] H.C. Rhim and O. Büyüköztürk. Electromagnetic properties of concrete at microwave frequency range. ACI Materials Journal, pages 262–271, 1998.

[4] A. Christ, A. Klingenböck, T. Samaras, C. Goiceanu, and N. Kuster. The dependence of electromagnetic far-field absorption on body tissue composition in the frequency range from 300 MHz to 6 GHz. IEEE Transactions on Microwave Theory and Techniques, 54(5):2188–2195, May 2006.